

CORRESPONDENCE

Open Access

SARS-CoV-2 Spike protein S2 subunit modulates γ -secretase and enhances amyloid- β production in COVID-19 neuropathy

Guanqin Ma¹, Deng-Feng Zhang^{1,2,3}, Qing-Cui Zou², Xiaochun Xie¹, Ling Xu^{1,2,3}, Xiao-Li Feng², Xiaohong Li¹, Jian-Bao Han², Dandan Yu^{1,2,3}, Zhong-Hua Deng², Wang Qu², Junyi Long², Ming-Hua Li²✉, Yong-Gang Yao^{1,2,3,4}✉ and Jianxiong Zeng^{1,2,3,5}✉

Dear Editor,

SARS-CoV-2-induced multi-lineage neural cell dysregulation has been documented¹. SARS-CoV-2 infection elevates neuroinflammation², alters brain structure³ leads to abnormal accumulation of neurodegenerative amyloid- β (A β) and phosphorylated tau^{4,5}, and increases the risk of cognitive impairment⁶ in COVID-19 patients. However, the mechanism underlying neurological dysfunctions following SARS-CoV-2 infection remains largely unknown.

To evaluate long-term impact of SARS-CoV-2 infection to the brain, the hACE2 transgenic mice as described previously⁷ were intranasally infected with a single low dose (1×10^2 TCID₅₀) of prototyped SARS-CoV-2 and maintained for up to 30 days post infection (dpi) (Fig. 1a). Presence of SARS-CoV-2 was found in cortex at 7 dpi but not at 30 dpi by the viral Spike protein immunostaining (Supplementary Fig. S1a). We found a remarkable activation of Iba1⁺ microglia and GFAP⁺ astrocytes in the hippocampus and cortex of infected mice at 30 dpi (Supplementary Fig. S1b–e), suggesting a persistent neuroinflammation. We looked for further brain changes by

analyzing transcriptomics of the hippocampal tissues at 30 dpi (Supplementary Fig. S2a). A series of dysregulated genes or pathways were identified in response to SARS-CoV-2 infection (Supplementary Table S1). Gene ontology analysis revealed that the upregulated genes were mainly enriched in pathways related to antiviral immune response and aging, while the downregulated genes were enriched in neuronal function-related pathways such as synaptic vesicle clustering (Fig. 1b). Specifically, the neuroinflammatory genes *Trem2*, *Ifitm3* and *Gfap* were significantly upregulated, whereas the neuronal genes *Map2* and *Synapsin II* (*Syn2*) were downregulated. Unexpectedly, mRNA levels of amyloid precursor protein (APP) processing-related genes such as *Bace1*, *Aph1*, *Presenilin 1* (*Psen1*), *Nicastrin* (*Ncstn*), and *Psenen* were unchanged (Fig. 1c). The upregulation of *Trem2* and *Gfap*, the downregulation of *Map2* and *Syn2*, and the un-alteration of *Bace1* and *Psen1* were validated by quantitative real-time PCR (Supplementary Fig. S2b). Such expression patterns were also observed in the brain transcriptomic dataset obtained from COVID-19 patients by single-nucleus RNA sequencing² (Supplementary Fig. S3a–c). These results suggest that the presence of the neurodegenerative hallmarks in COVID-19 brain might not be regulated at the transcriptional level but through an unknown regulatory mechanism.

To explore potential mechanisms underlying COVID-19-related neuropathology, we tested whether SARS-CoV-2 membrane protein plays a role in this process. The γ -secretase complex, comprising PEN-2, APH-1, PS1 and NCT, is a critical membrane complex contributing to A β production in Alzheimer's disease (AD) pathogenesis⁸. Initially, we conducted co-immunoprecipitation (co-IP) in

Correspondence: Ming-Hua Li (limh@mail.kiz.ac.cn) or Yong-Gang Yao (yaoyg@mail.kiz.ac.cn) or Jianxiong Zeng (zengjianxiong@mail.kiz.ac.cn)

¹Key Laboratory of Animal Models and Human Disease Mechanisms of the Chinese Academy of Sciences, and KIZ-CUHK Joint Laboratory of Bioresources and Molecular Research in Common Diseases, Kunming Institute of Zoology, Chinese Academy of Sciences, Kunming, Yunnan, China

²Kunming National High-level Biosafety Research Center for Non-Human Primates, Center for Biosafety Mega-Science, Kunming Institute of Zoology, Chinese Academy of Sciences, Kunming, Yunnan, China

Full list of author information is available at the end of the article

These authors contributed equally: Guanqin Ma, Deng-Feng Zhang, Qing-Cui Zou, Xiaochun Xie

© The Author(s) 2022



Open Access This article is licensed under a Creative Commons Attribution 4.0 International License, which permits use, sharing, adaptation, distribution and reproduction in any medium or format, as long as you give appropriate credit to the original author(s) and the source, provide a link to the Creative Commons license, and indicate if changes were made. The images or other third party material in this article are included in the article's Creative Commons license, unless indicated otherwise in a credit line to the material. If material is not included in the article's Creative Commons license and your intended use is not permitted by statutory regulation or exceeds the permitted use, you will need to obtain permission directly from the copyright holder. To view a copy of this license, visit <http://creativecommons.org/licenses/by/4.0/>.

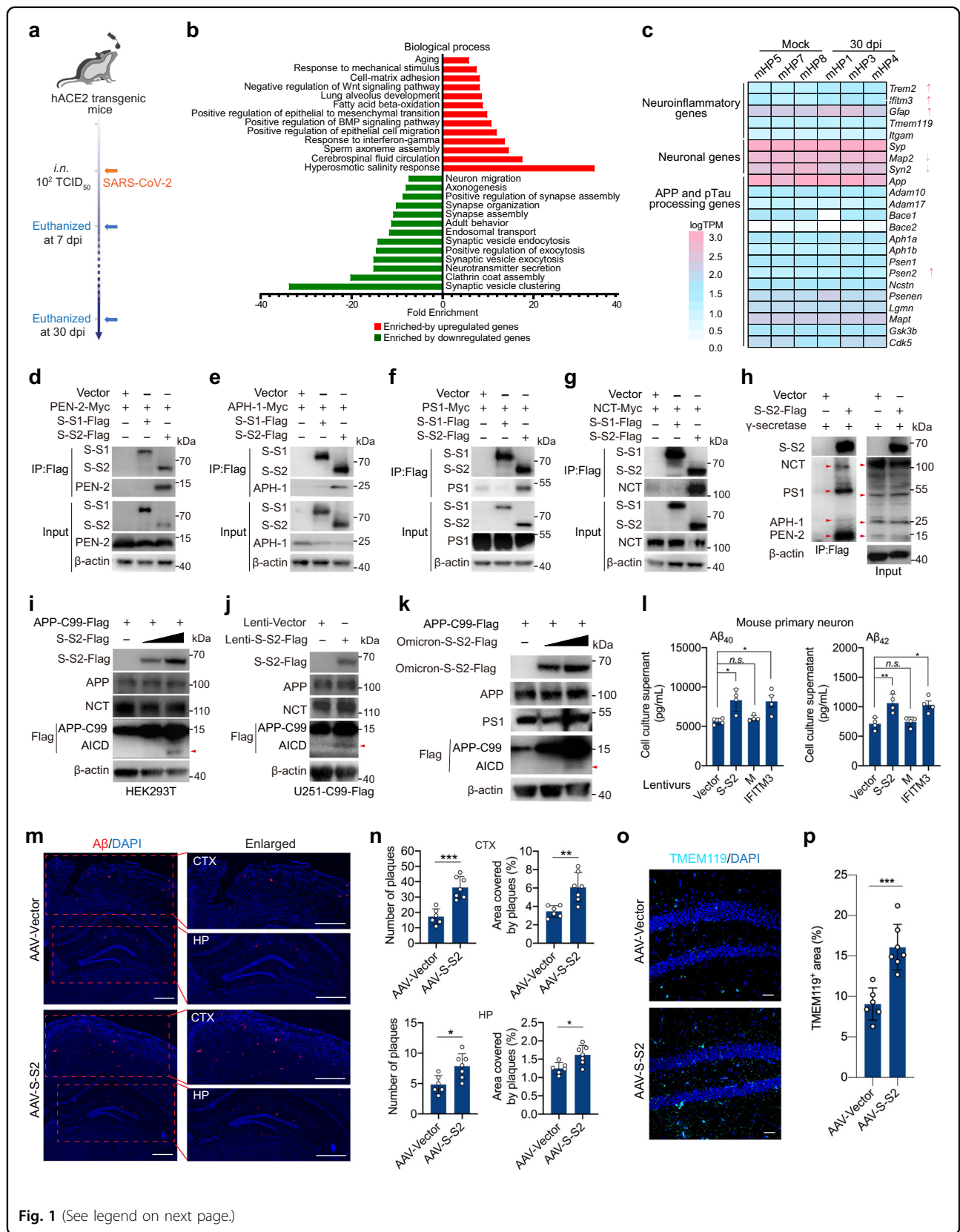


Fig. 1 (See legend on next page.)

(see figure on previous page)

Fig. 1 SARS-CoV-2 Spike protein S2 subunit binds to and modulates γ -secretase to enhance A β production. **a** hACE2 transgenic mice were intranasally (i.n.) infected by prototyped SARS-CoV-2. Brain cortical or hippocampal tissues were collected for immunofluorescence (7 or 30 dpi) and RNA-seq analysis (30 dpi). **b** Enrichment analysis of representative biological processes in the hippocampal RNA-seq data at 30 dpi in **a**. **c** Expression pattern of representative genes within the categorized gene ontology as indicated. **d–g** co-IP assays of anti-flag monoclonal antibody in HEK293T cells transfected with vector, S-S1-flag or S-S2-flag, together with myc-tagged PEN-2 (**d**), APH-1 (**e**), PS1 (**f**), and NCT (**g**). **h** co-IP assays of anti-flag monoclonal antibody in HEK293T cells co-transfected with myc-tagged PEN-2, APH-1, PS1 and NCT, together with S-S2-flag. **i** HEK293T cells were transfected with expression vector of APP-C99 with C-terminal flag tag (0.5 μ g) and increasing amount of prototyped S-S2-Flag (0, 0.25, and 0.5 μ g) in 12-well plates for 36 h. **j** U251-C99 cells were transfected with lentivirus carrying prototyped S-S2-Flag in 12-well plates for 36 h. The production of AICD (red arrows) in **i** and **j** was examined by immunoblot analysis. **k** HEK293T cells were co-transfected with expression vector of APP-C99 with C-terminal flag tag (APP-C99-Flag, 0.5 μ g) and increasing amount (0, 0.25 or 0.5 μ g) of Omicron S-S2-Flag in 12-well plates for 36 h. The production of AICD (red arrow) from APP-C99 was detected by immunoblot analysis. **l** Mouse primary neurons were isolated from embryonic (E18.5) brains and cultured in 24-well plates. Neurons were transfected with lentivirus carrying empty vector (vector), prototyped S-S2, M, or IFITM3 for 36 h. The A β 40 (left) and A β 42 (right) levels in the supernatants were quantified by ELISA. Means \pm SD; $n = 4$; n.s., not significant; * $P < 0.05$; ** $P < 0.01$, one-way ANOVA with Bonferroni's post hoc test. **m** Representative anti-A β antibody staining of cortical (CTX) and hippocampal (HP) sections in APP/PS1 Δ E9 mice with AAV delivery of prototyped S-S2 (AAV-S-S2) and AAV control (AAV-Vector). Scale bar, 500 μ m. **n** Quantitative analysis of the number of A β plaques and the percentage of area covered by A β plaques in cortical (upper) and hippocampal (bottom) tissues in **m**. Each slide was counted for A β plaque number and A β plaque area via ImageJ software, and the percentage of the plaque area was calculated. **o** Representative immunofluorescence of microglial marker TMEM119 protein in hippocampal sections of AAV-S-S2 or AAV-Vector. Scale bar, 30 μ m. **p** Quantification of percentage of TMEM119⁺ area in **o**. Statistical analyses for **n** and **p**, Means \pm SD; $n = 6$ (AAV-Vector group) or $n = 7$ (AAV-S-S2 group); * $P < 0.05$; ** $P < 0.01$; *** $P < 0.001$, Student's *t*-test.

HEK293T cells and found that SARS-CoV-2 Spike S2 subunit (S-S2), but not S-S1 protein, interacted individually with PEN-2 (Fig. 1d), APH-1 (Fig. 1e), PS1 (Fig. 1f) and NCT (Fig. 1g), and even bound to all these four components (Fig. 1h). The inverse co-IP could validate the interactions between S-S2 and PS1 or NCT (Supplementary Fig. S4a, b). To determine whether C-terminal transmembraneTM domain in S-S2 constitutes the structural basis for its interaction with γ -secretase, we examined membrane (M) protein of SARS-CoV-2 but found no interaction with PEN-2 and PS1 (Supplementary Fig. S4c, d), suggesting a specific interaction between S-S2 and γ -secretase. We next performed glutathione *s*-transferase (GST) pull-down and found that S-S2 can directly bind to PS1 and NCT (Supplementary Fig. S4e, f). Immunocytochemistry assay showed the co-localization of S-S2 with γ -secretase components individually in Hela cells (Supplementary Fig. S4g–j) and in the brain sections of infected mice at 7 dpi (Supplementary Fig. S4k).

SARS-CoV-2 Omicron variant (BA.1) Spike S2 subunit possesses six mutations (N764K, D796Y, N856K, Q954H, N969K, and L981F) compared to the prototype⁹. To see whether these mutations would interfere with its interaction with γ -secretase, co-IP assay in HEK293T cells showed that Omicron S-S2 not only interacted efficiently with PS1 and NCT (Supplementary Fig. S5a, b), but also had a comparable binding capacity to PS1 and NCT as prototyped S-S2 (Supplementary Fig. S5c, d), suggesting Omicron BA.1 S-S2 is capable of binding to γ -secretase.

An enzymatic cleavage of the APP by both β -secretase and γ -secretase, acting together, produces A β , which can cause widespread neuropathy within brain and is a pathological hallmark of AD¹⁰. The cleavage site of γ -secretase is located on C-terminal APP, namely APP

C-terminal 99 fragment (APP-C99) only contains the cleavage site of γ -secretase. As a result, APP intracellular domain (AICD) at C-terminal C99 domain is produced by γ -secretase cleavage¹¹. To examine whether the interaction between S-S2 and γ -secretase modulates the cleavage activity, we initially detected the production of AICD. Immunoblot showed that prototyped S-S2 promoted the production of flag-tagged AICD, whereas the expression of APP and NCT was largely unchanged (Fig. 1i). This was validated by the observation of the increased production of flag-tagged AICD in U251-C99 cells while the expression of APP and NCT was largely unaltered (Fig. 1j). Similarly, Omicron S-S2 also increased the production of flag-tagged AICD, while the expression of APP and PS1 was unchanged (Fig. 1k). These results demonstrate that the increased production of AICD from the APP cleavage was caused by S-S2 modulation of γ -secretase.

HEK-APP695¹² cells transfected with prototyped S-S2, but not the M, produced higher level of A β 40 than non-transfected cells via enzyme-linked immunosorbent assay (ELISA), while a similar increase of A β 40 was also observed upon the transfection of IFITM3 as a positive control¹³ (Supplementary Fig. S6a). To further evaluate this effect, we used neuronal cells including U251 and mouse primary neurons, both endogenously expressing APP protein. Lentiviral transduction of prototyped S-S2 or IFITM3 invariably caused the increase of A β 40 or A β 42 production as compared to empty-vector lentivirus transduction in U251 cells (Supplementary Fig. S6b) and mouse primary neurons (Fig. 1l), whereas lentiviral transduction of the M did not have such an effect. As expected, mouse primary neurons transfected with lentiviral Omicron-S-S2 produced higher A β 40 and A β 42 levels (Supplementary Fig. S6c). These results demonstrate

that SARS-CoV-2 Spike S2 subunit can modulate γ -secretase to increase A β production.

To investigate whether S-S2 modulates γ -secretase *in vivo*, we examined hippocampal and cortical tissues of APP^{sw}/PSEN1 Δ E9 (hereafter referred to as APP/PS1 Δ E9) mice, which have mutated human APP (Swedish mutations K595N/M596L) and the human PSEN1/PS1 lacking exon 9¹⁴, 2 months after AAV delivery of S-S2. Immunohistochemistry showed a widespread overexpression of S-S2 in hippocampal tissues (Supplementary Fig. S7a). Measurement of soluble and insoluble A β levels using ELISA showed that soluble A β 42 species, but not insoluble A β 40 and A β 42 and soluble A β 40, were markedly increased in cortical tissues of APP/PS1 Δ E9 mice with S-S2 overexpression relative to empty vector group (Supplementary Fig. S7b–e). Similarly, immunostaining showed a significant increase of A β burden in cortical and hippocampal tissues of APP/PS1 Δ E9 mice after S-S2 delivery (Fig. 1m). The delivery of S-S2 increased the A β plaque-deposited area in cortical and hippocampal tissues of APP/PS1 Δ E9 mice (Fig. 1n). Overall, overexpression of SARS-CoV-2 S-S2 in hippocampus exacerbated A β burden in APP/PS1 Δ E9 mice.

Neuroinflammation, an important factor in AD pathogenesis, promotes A β pathology¹⁵. A significant increase of Iba1⁺ microglia and GFAP⁺ astrocytes (Supplementary Fig. S8a–c) was observed in hippocampal tissues of APP/PS1 Δ E9 mice after delivery of S-S2. Staining of microglial marker TMEM119 validated the elevated neuroinflammation following S-S2 delivery (Fig. 1o, p). These results demonstrated that S-S2 overexpression increased A β deposit and caused neuroinflammation in A β pathology of APP/PS1 Δ E9 mice. Both the area covered by NeuN-labeled neuronal cells and the thickness of NeuN-labeled CA1 subfield (Supplementary Fig. S8d–f) were not significantly altered in hippocampal tissues following S-S2 delivery, suggesting that S-S2 overexpression might not cause neuronal loss after AAV delivery for 2 months.

In summary, we have identified S-S2 subunit as a γ -secretase modulatory protein and revealed a previously unknown mechanistic insight into COVID-19-related neuropathological sequelae (Supplementary Fig. S9). A systematical examination of multiple Omicron subvariants (Supplementary Fig. S10) on potential brain dysfunction would be inspired in future studies. The Spike protein could function as an immune switch to increase γ -secretase activity and A β production and contribute to neurological changes in COVID-19 patients.

Acknowledgements

We thank Dr. Chang-Wen Ke from Guangdong Provincial Center for Disease Control and Prevention for providing SARS-CoV-2 strain. We thank Dr. Xin He from Sun Yat-Sen University for giving Omicron Spike plasmid and Dr. Jing Sun from Guangzhou Medical University for offering prototyped Spike plasmid. We also thank Figdraw (www.figdraw.com) for the assistance in

creating diagram. This work was supported by the Ministry of Science and Technology of China (2022ZD0213500), Yunnan Province (202201AW070020, 2019FA009 and 2019F01015), the National Natural Science Foundation of China (31730037, 82022017, 31970965), the Bureau of Frontier Sciences and Education, Chinese Academy of Sciences (CAS) (QYZDJ-SSW-SMC005), the key project of the CAS “Light of West China” Program, the Strategic Priority Research Program (B) of the CAS (XDB02020003), and CAS Youth Innovation Promotion Association.

Author details

¹Key Laboratory of Animal Models and Human Disease Mechanisms of the Chinese Academy of Sciences, and KIZ-CUHK Joint Laboratory of Bioresources and Molecular Research in Common Diseases, Kunming Institute of Zoology, Chinese Academy of Sciences, Kunming, Yunnan, China. ²Kunming National High-level Biosafety Research Center for Non-Human Primates, Center for Biosafety Mega-Science, Kunming Institute of Zoology, Chinese Academy of Sciences, Kunming, Yunnan, China. ³Kunming College of Life Science, University of Chinese Academy of Sciences, Kunming, Yunnan, China. ⁴CAS Center for Excellence in Brain Science and Intelligence Technology, Chinese Academy of Sciences, Shanghai, China. ⁵Yunnan Key Laboratory of Biodiversity Information, Kunming Institute of Zoology, Chinese Academy of Sciences, Kunming, Yunnan, China

Author contributions

All authors read and approved the final version of the manuscript. J.Z., Y.G.Y., and M.H.L. conceived of the research and designed the study. J.Z. and Y.G.Y. wrote the manuscript. G.M., D.F.Z., Q.C.Z., X.X., L.X., X.L., J.B.H., X.L.F., D.Y., Z.H.D., W.Q., and J.L. performed the experiments or discussed the data. D.F.Z. analyzed the RNA-seq data. All authors commented on the manuscript.

Data availability

The hippocampal RNA-seq data were deposited in the NCBI GEO database under the accession number GSE199545.

Conflict of interest

The authors declare no competing interests.

Publisher's note

Springer Nature remains neutral with regard to jurisdictional claims in published maps and institutional affiliations.

Supplementary information The online version contains supplementary material available at <https://doi.org/10.1038/s41421-022-00458-3>.

Received: 24 June 2022 Accepted: 12 August 2022

Published online: 30 September 2022

References

1. Fernandes-Castaneda, A. et al. Mild respiratory COVID can cause multi-lineage neural cell and myelin dysregulation. *Cell* <https://doi.org/10.1016/j.cell.2022.06.008> (2022).
2. Yang, A. C. et al. Dysregulation of brain and choroid plexus cell types in severe COVID-19. *Nature* **595**, 565–571 (2021).
3. Douaud, G. et al. SARS-CoV-2 is associated with changes in brain structure in UK Biobank. *Nature* **604**, 697–707 (2022).
4. Frontera, J. A. et al. Comparison of serum neurodegenerative biomarkers among hospitalized COVID-19 patients versus non-COVID subjects with normal cognition, mild cognitive impairment, or Alzheimer's dementia. *Alzheimers Dement.* **18**, 899–910 (2022).
5. Shen, W. B. et al. SARS-CoV-2 invades cognitive centers of the brain and induces Alzheimer's-like neuropathology. *bioRxiv* <https://doi.org/10.1101/2022.01.31.478476> (2022).
6. Liu, Y. H. et al. Post-infection cognitive impairments in a cohort of elderly patients with COVID-19. *Mol. Neurodegener.* **16**, 48 (2021).
7. Zeng, J. et al. Specific inhibition of the NLRP3 inflammasome suppresses immune overactivation and alleviates COVID-19 like pathology in mice. *eBioMedicine* **75**, 103803 (2022).

8. Sisodia, S. S. & St George-Hyslop, P. γ -Secretase, notch, A β and alzheimer's disease: where do the presenilins fit in? *Nat. Rev. Neurosci.* **3**, 281–290 (2002).
9. Mannar, D. et al. SARS-CoV-2 Omicron variant: Antibody evasion and cryo-EM structure of spike protein-ACE2 complex. *Science* **375**, 760–764 (2022).
10. O'Brien, R. J. & Wong, P. C. Amyloid precursor protein processing and Alzheimer's disease. *Annu. Rev. Neurosci.* **34**, 185–204 (2011).
11. Knopman, D. S. et al. Alzheimer disease. *Nat. Rev. Dis. Prim.* **7**, 33 (2021).
12. Hung, A. Y., Koo, E. H., Haass, C. & Selkoe, D. J. Increased expression of beta-amyloid precursor protein during neuronal differentiation is not accompanied by secretory cleavage. *Proc. Natl. Acad. Sci. USA* **89**, 9439–9443 (1992).
13. Hur, J. Y. et al. The innate immunity protein IFITM3 modulates gamma-secretase in Alzheimer's disease. *Nature* **586**, 735–740 (2020).
14. Jankowsky, J. L. et al. Mutant presenilins specifically elevate the levels of the 42 residue beta-amyloid peptide in vivo: evidence for augmentation of a 42-specific gamma secretase. *Hum. Mol. Genet.* **13**, 159–170 (2004).
15. Pascoal, T. A. et al. Microglial activation and tau propagate jointly across Braak stages. *Nat. Med.* **27**, 1592–1599 (2021).

Supplementary Information

SARS-CoV-2 Spike protein S2 subunit modulates γ -secretase and enhances amyloid- β production in COVID-19 neuropathy

Guanqin Ma^{1,6}, Deng-Feng Zhang^{1,2,3,6}, Qing-Cui Zou^{2,6}, Xiaochun Xie^{1,6}, Ling Xu^{1,2,3}, Xiao-Li Feng², Xiaohong Li¹, Jian-Bao Han², Dandan Yu^{1,2,3}, Zhong-Hua Deng², Wang Qu², Junyi Long², Ming-Hua Li^{2,*}, Yong-Gang Yao^{1,2,3,4,*}, Jianxiong Zeng^{1,2,3,5,*}

¹Key Laboratory of Animal Models and Human Disease Mechanisms of the Chinese Academy of Sciences, and KIZ-CUHK Joint Laboratory of Bioresources and Molecular Research in Common Diseases, Kunming Institute of Zoology, Chinese Academy of Sciences, Kunming, Yunnan 650201, China

²Kunming National High-level Biosafety Research Center for Non-Human Primates, Center for Biosafety Mega-Science, Kunming Institute of Zoology, Chinese Academy of Sciences, Kunming, Yunnan 650107, China

³Kunming College of Life Science, University of Chinese Academy of Sciences, Kunming, Yunnan 650204, China

⁴CAS Center for Excellence in Brain Science and Intelligence Technology, Chinese Academy of Sciences, Shanghai 200031, China

⁵Yunnan Key Laboratory of Biodiversity Information, Kunming Institute of Zoology, Chinese Academy of Sciences, Yunnan, 650201, China

⁶These authors contributed equally

*Corresponding authors:

Ming-Hua Li (limh@mail.kiz.ac.cn)

Yong-Gang Yao (yaoyg@mail.kiz.ac.cn)

Jianxiong Zeng (zengjianxiong@mail.kiz.ac.cn)

Materials and Methods

Cells

HEK293T, Vero E6, Hela, and U251 cells were obtained from the Kunming Cell Bank, Kunming Institute of Zoology (KIZ), and were grown in Dulbecco's Modified Eagle medium (DMEM) high glucose supplemented with 10% FBS, 1% penicillin/streptomycin at 37°C in humidified 5% CO₂ and 95% air. Mouse primary neurons were isolated and cultured as described previously¹. Briefly, cerebral cortices from E18.5 mouse embryos were dissected, carefully stripped of their meninges, digested with TrypLE Express Enzyme (Catalog # 12604013; ThermoFisher Scientific) with RQ1 RNase-free DNase (Catalog # M6101; Promega) for 20 min at 37°C, and dispersed to single-cell level by passing through a 70 µm cell strainer. The cell suspension was then cultured with Neurobasal medium supplemented with B27 Supplement (Catalog # 17504044; ThermoFisher Scientific) at 37°C in humidified 5% CO₂, 95% air on poly-D-Lysine (Catalog # P0899; Millipore) pre-coated coverslips in 12-well culture plates. Half the medium was replaced on alternate days.

Virus

The SARS-CoV-2 strain was kindly provided by Guangdong Provincial Center for Disease Control and Prevention, Guangdong Province of China and was described in our previous studies^{2,3}. The virus was propagated and titrated in Vero E6 cells, which were cultured in DMEM supplemented with 2% FBS. The viral sequence is accessible in the China National Microbiology Data Center (Accession No. NMDCN0000HUI).

Plasmids

Human presenilin-1 (PS1), nicastrin (NCT), anterior pharynx-defective 1 (APH-1), or presenilin enhancer 2 (PEN-2) were cloned into pCAGGS vector with a C-terminal myc tag. Prototyped SARS-CoV-2 full-length spike, Spike S1 subunit (S-S1), Spike S2 subunit (S-S2), membrane (M), Omicron BA.1 lineage Spike S2 subunit (Omicron S-S2) and human IFITM3 were cloned into pCAGGS vector

with a C-terminal flag tag. Human APP695, APP-C99, prototyped SARS-CoV-2 Spike S1 subunit, Spike S2 subunit, and Omicron Spike S2 subunit were cloned into lentiviral pCDH-CMV-MCS-EF1-Puro vector with a C-terminal flag tag. Prototyped SARS-CoV-2 Spike S2 subunit was also cloned into bacterial pGEX-6p-1 vector with a N-terminal GST tag.

Glutathione-S-transferase (GST) pull-down

For expression and purification of recombinant GST-fusion proteins, GST-S-S2 and the negative control GST protein were expressed in *E. coli* strain BL21 (DE3) at 25°C in the presence of 0.5 mM Isopropyl β-D-1-thiogalactopyranoside (IPTG). Cell pellets were resuspended in GST lysis buffer (150 mM NaCl, 1mM EDTA [pH 8.0], 20 mM Tris-Cl [pH 8.0] supplemented with 1% Triton X-100 and protease inhibitor cocktail (Catalog # K1007; Apexbio), followed by sonication, and the cell debris was removed by centrifugation (13,500 rcf at 4°C) for 30 min. The proteins in the supernatant were purified by glutathione Sepharose (Catalog # HY-K0234; MedChemExpress) accordingly to the manufacturer's protocol and the purified proteins were quantified by a UV-visible spectrophotometer and the BCA protein assay kit (Catalog # P0010S; Beyotime). Purified GST-fusion proteins with the same amount were incubated with HEK293T cell lysates overnight and were then washed with the GST lysis buffer five times followed by Western immunoblotting analysis.

Co-immunoprecipitation

Cultured cells were lysed with RIPA lysis buffer (Catalog # P0013C; Beyotime) supplemented with 1% CHAPSO (Catalog # C3649; Millipore) and protease inhibitor cocktail (Catalog # K1007; Apexbio). After clarification and preclearing, protein amounts were quantified by the BCA protein assay kit (Catalog # P0010S; Beyotime). Around 1/10 volume of cell lysates was heated as whole cell lysates in Western blot analysis and the remaining 9/10 volume of the lysates was incubated with anti-flag magnetic beads (Catalog # HY-K0207; MedChemExpress) or anti-myc magnetic beads (Catalog # HY-K0206;

MedChemExpress) for 16 h at 4°C. Immune complexes were washed with the lysis buffer and subjected to Western blot analysis.

γ -secretase activity measurement

HEK293T-APP695, U251 cells, or mouse primary neurons were co-transfected with expression vector for prototyped S-S2, M, Omicron S-S2, or IFITM3, or transduced with lentiviral prototyped S-S2, M, or Omicron S-S2. It should be noted that U251⁴ and primary neurons⁵ endogenously express APP. The cell culture supernatants were collected for enzyme-linked immunosorbent assay (ELISA) at 36 h post transfection or transduction. HEK293T-C99 were transfected with increased amount expression vector of prototyped S-S2 or Omicron S-S2, and U251-C99 cells were transduced with lentiviral prototyped S-S2. The resulting cell lysates were collected for Western blot at 36 h post transfection or transduction.

The resulting supernatants from cell cultures were collected and the concentrations of A β 40/A β 1-40 and A β 42/A β 1-42 were determined by using human A β 40 kit (Catalog # E-EL-H0542c; Elabscience), human A β 42 kit (Catalog # E-EL-H0543c; Elabscience), mouse A β 40 kit (Catalog # E-EL-M3009; Elabscience), and mouse A β 42 kit (Catalog # E-EL-M3010; Elabscience), respectively, following the manufacturer's protocols.

RNA-sequencing of hippocampal tissues from mouse model of SARS-CoV-2 infection

We performed RNA-sequencing (RNA-seq) of hippocampal tissues from mice with and without SARS-CoV-2 infection. Total RNA (1.5 μ g) per sample was used for the library preparation. Sequencing libraries were constructed using the NEBNext UltraTM RNA Library Prep kit for Illumina (NEB, USA) following the manufacturer's instructions. Libraries were sequenced on an Illumina Nova seq platform and 150 bp paired-ends reads were generated. Sequencing reads were processed and differential gene expression analysis was performed according to standard protocols as described in our previous studies^{6,7}. In brief, the raw reads were trimmed to remove sequencing adapters and low-quality reads with Trimmomatic⁸. The clean reads were aligned to the standard mouse reference genome (GRCm38) using

STAR⁹. RSEM¹⁰ was then used to count aligned reads that mapped to the annotated mouse genes. Gene-level differential expression analyses were performed using R package DESeq2¹¹. Gene Ontology biological processes enrichment analysis for differentially expressed genes was performed using clusterProfiler¹².

Cell type specific transcriptomic analysis of A β processing genes using single-nucleus RNA-seq data from cortex tissues of COVID-19 patients

To investigate whether the A β processing genes were altered in cortical tissues of patients with COVID-19, and whether the differential expression was cell-type specific, we retrieved one reported single-cell RNA-seq dataset. The dataset contains 38,217 single-nucleus gene expression profiles from the medial frontal cortex of 8 controls and 8 COVID-19 patients¹³, with normalized counts data; and was downloaded from https://twc-stanford.shinyapps.io/scRNA_Brain_COVID19. The data was processed using Seurat¹⁴ and a violin plot was generated for each gene of interest grouped by cell-types and infection status.

Animal models

8-12 weeks old male hACE2 transgenic mice were purchased from the Shanghai Model Organisms as described previously¹⁵. After being anesthetized with isoflurane (RWD Life Science), the mice were intranasally infected with a total of 20 μ L containing 1×10^2 median tissue culture infectious Dose (TCID₅₀) of live SARS-CoV-2 in the animal biosafety level 3 laboratory (ABSL-3) of the KIZ. At the indicated time points post infection, tissue samples were collected from the animals after euthanasia and stored in -80°C freezer (for RNA extraction) or in 4% paraformaldehyde (PFA; for immunofluorescence).

Animals were maintained on a 12-h light/dark cycle, with free access to food and water. All these experiments with live SARS-CoV-2 were performed in the ABLS3 laboratory of the KIZ. The Institutional Animal Care and Use Committee of KIZ approved all experimental procedures and protocols used in this study (Approval No. IACUC-RE-2021-05-009).

Stable cell lines

HEK293T or U251 cells stably overexpressing APP695 or APP-C99 were generated by lentiviral transduction. Briefly, the lentivirus was made by co-transfection of lentiviral transfer vector carrying APP695 (GenBank: A33292.1) or APP-C99 coding sequence (pCDH-CMV-MCS-EF1-Puro) and packaging plasmids pMD2G (Catalog # 12259; Addgene) and psPAX2 (Catalog # 12260; Addgene) into HEK293T cells using Lipofectamine 3000 (Catalog # L3000015; ThermoFisher Scientific). The lentivirus-containing supernatants were collected and pooled at 72 h post-transfection. HEK293T or U251 cells were transduced by the lentivirus at 1:1 dilution of culture medium and lentivirus-containing supernatant in the presence of 8 $\mu\text{g}/\text{mL}$ polybrene (Millipore). The stable cells overexpressing APP695 or APP-C99 were selected and maintained in growth medium with 1 $\mu\text{g}/\text{mL}$ puromycin (InvivoGen).

Quantitative real-time PCR (qRT-PCR)

Total RNA was extracted from homogenized brain tissues using a TRIzol reagent (ThermoFisher Scientific). Target transcripts were determined by qRT-PCR using qScriptTM One-Step qRT-PCR kit (Catalog # 95057-050; Quanta Biosciences) on CFX96 real-time PCR system (Bio-Rad). The primer sequences are listed in Supplementary Table 2.

Immunofluorescence

Immunofluorescence was performed as described in our previous studies^{15,16}. Briefly, brain slides between bregma -1.8 mm and -2.2 mm were prepared via frozen sections for each animal. For antigen retrieval, slides were immersed in a quick antigen retrieval solution (P0090, Beyotime). Then slides were washed with 1 \times phosphate-buffered saline (PBS; pH 7.4), and blocked with 5% bovine serum albumin (BSA) in 1 \times PBST (0.3% Triton-X 100 in PBS) at 37°C for 60 min. The primary antibodies used are listed in Supplementary Table 3. The primary antibodies above were diluted in 3% donkey serum) in 1 \times

PBST (0.2% Triton-X 100) and incubated overnight at 4°C. Slides were then washed, and immunoreactivity was detected using Donkey anti-Rabbit IgG Highly Cross-Adsorbed Secondary Antibody, Alexa Fluor Plus 488, Donkey anti-Mouse IgG Highly Cross-Adsorbed Secondary Antibody, Alexa Fluor Plus 555, Donkey anti-Rat IgG Highly Cross-Adsorbed Secondary Antibody, Alexa Fluor Plus 647 (1:500; ThermoFisher Scientific) for 1 h at room temperature. Slides were counterstained with 5 µg/mL 4',6-diamidino-2-phenylindole (DAPI; ThermoFisher Scientific) for 10 min at room temperature and washed with 1 × PBST (0.2% Triton-X 100) three times. Slides were visualized using ZEISS LSM 880 confocal microscope. The digital images were imported into ImageJ software in which the area of targeted signals was automatically analyzed, and the percentage of target signal was calculated.

Immunoblotting

Immunoblotting was performed as described previously^{15,17}. In brief, protein samples were separated by SDS-PAGE and transferred to PVDF membrane by semi-dry transfer at 25 V for 30 min. The membrane was blocked in 5% skim milk in 1 × PBST for 1 h and incubated overnight with commercial primary antibody in 5% bovine serum albumin (BSA) at 4°C. The membrane was incubated with anti-mouse or anti-rabbit HRP-conjugated secondary antibodies in 5% milk and bands were developed with Chemi-Doc XRS imaging (Bio-Rad). The primary antibodies used are listed in Supplementary Table 3.

Adenovirus associated virus (AAV) mediated gene delivery and tissue analyses

5-month-old APP/PS1ΔE9 mice¹⁸ were used for AAV-mediated gene delivery as described previously¹⁹. Briefly, the recombinant AAV php.eb vectors, with GFP expression carrying empty vector (AAV-Vector) or SARS-CoV-2 Spike S2 subunit (AAV-S-S2) were developed. The purified viruses were stored at -80°C and diluted with saline to 1 × 10¹³ vector genomes (vg)/mL for injection. The mice were anesthetized by intraperitoneal injection of Zoletil-50 (80 mg/kg body weight) with xylazine (20 mg/kg body weight) and positioned on a stereotactic frame (Panlab, Harvard, MA, USA), then each animal was bilaterally injected with 1 µL viral solution (equivalent to 1 × 10¹⁰ vg) into the hippocampus (stereotaxic

coordinates: anteroposterior, -2 mm; mediolateral, ± 2.1 mm; dorsoventral, -1.9 mm) with a syringe pump (Panlab, Harvard, MA, USA) at a speed of 200 nL/min. The needle was left in place for an additional 5 min before being slowly removed. The mice were maintained at the experimental animal core facility of KIZ on a 12-h light/dark cycle, with free access to food and water. The effects of AAV-Vector and AAV-S-S2 on neurological outcomes in the mice were assessed at 2 months post injection. The animals were euthanized prior to the collection of brain tissues. Briefly, the brain was carefully removed and rinsed in cold PBS, followed by immediate dissection into two halves. A part of cortex was stored at -80°C for the biochemical assays, whereas the rest of the tissues were fixed in 4% paraformaldehyde in PBS at 4°C for the immunofluorescence assays.

We isolated plaque-related insoluble and soluble A β using the protocols described in our previous studies^{19,20}. In brief, each sample of cortical tissue was weighed and then homogenized with 100 μL of RIPA lysis buffer (Catalog # P0013; Beyotime) containing protease inhibitor (Catalog # K1007; Apexbio) and phosphatase inhibitors (Catalog # HY-K0023; MedChemExpress) on ice, followed by centrifugation at 13,000 g for 15 min at 4°C , before collecting the supernatants and pellets. The protein concentrations of the supernatants were measured by using the BCA protein assay kit (Catalog # P0010S; Beyotime) and were adjusted to the same concentration for quantifying the soluble A β concentration by ELISA. The pellets were resuspended in a volume of 100 μL of RIPA lysis buffer, followed by centrifugation at 13,000 g for 15 min at 4°C to remove potential soluble A β . This washing step was repeated 3 times to remove all soluble A β . Then, the pellets containing insoluble A β were solubilized in sodium dodecyl sulfate (SDS) buffer (2% SDS, 25 mM Tris-HCl, pH 7.4). After pulsed sonication for 15 sec, the SDS fractions were quantified for protein concentrations and processed for measuring insoluble A β concentration, using the same procedure for soluble A β . The levels of A β 40 and A β 42 in mouse cortex tissues were determined by using the A β 40 kit (Catalog # E-EL-H0542c; Elabscience) and A β 42 kit (Catalog # E-EL-H0543c; Elabscience), respectively, following the manufacturer's protocols. Although a recent event challenged the association between A β and Alzheimer's disease²¹, the involvement of A β species A β 40 and A β 42 as indicators as neural cell dysregulation has not been questioned²²⁻²⁵. Therefore,

we used the levels of A β 40 and A β 42 as a valid indicator for potential degeneration of brain during the development of Alzheimer's disease.

Statistical analysis

All appropriate data were analyzed using GraphPad Prism 8 (GraphPad Software Inc.). All hypothesis tests were performed as two-tailed tests. Specific statistical analysis methods were described in the related figure legends where results are presented. Values were considered statistically significant for p values < 0.05.

Supplementary Figures

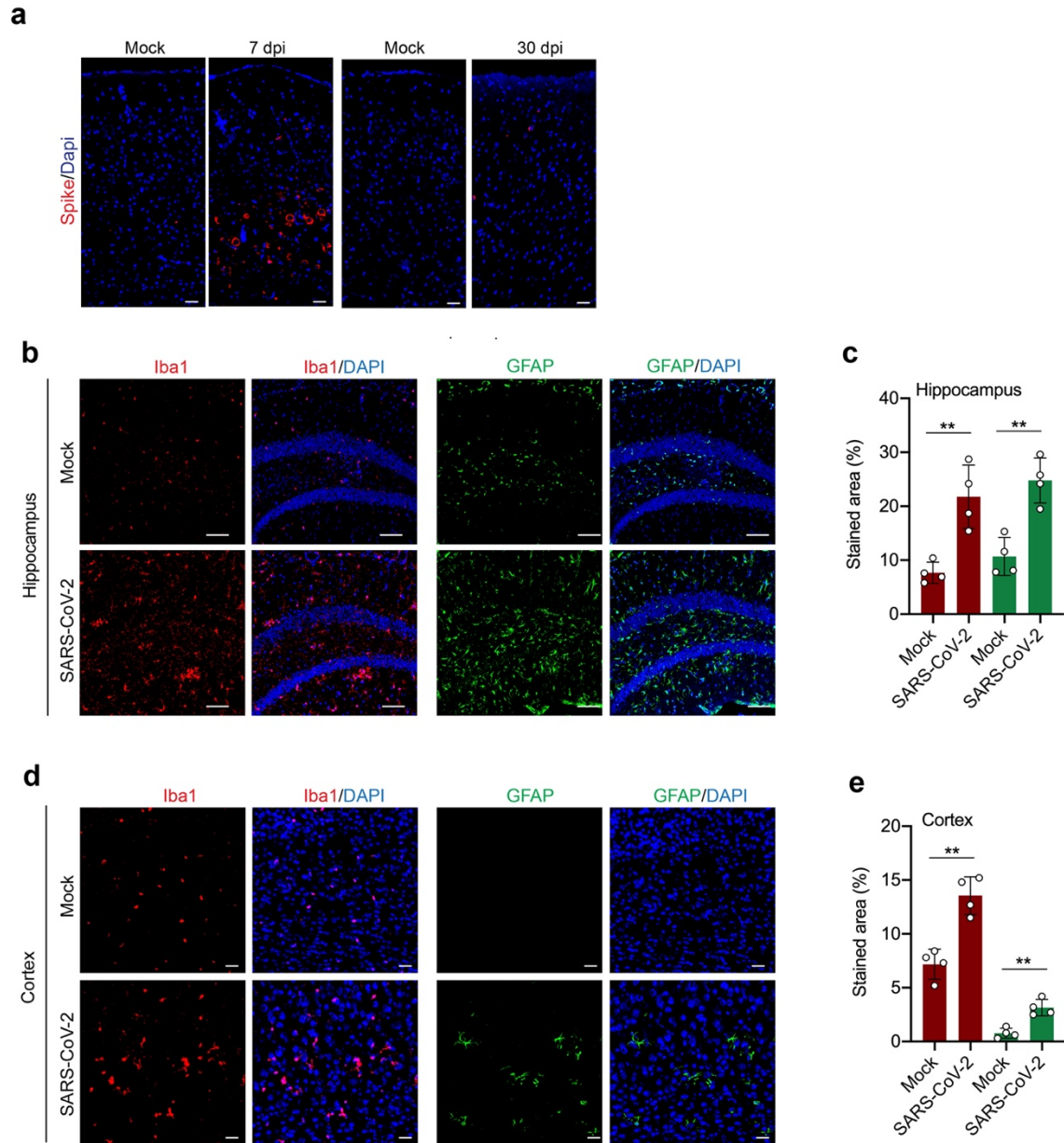


Fig. S1 Activation of glial cells in brain sections of SARS-CoV-2-infected hACE2 transgenic mice
a Representative immunofluorescence of SARS-CoV-2 Spike protein in cortical sections from infected mice at 7 dpi and 30 dpi and uninfected (mock) mice at the corresponding time points. Scale bar, 30 μ m.
b Representative immunofluorescence of microglial Iba1 (*left*) and astrocytic GFAP (*right*) of hippocampal area in mouse brain sections at 30 dpi. Scale bar, 30 μ m. **c** Quantification of percentage of Iba1⁺ (red) and GFAP⁺ (green) area in **b**. Each slide was used and counted for stained area via ImageJ software, and the percentage of average of stained area each section was calculated. **d** Representative immunofluorescence of microglial Iba1 (*left*) and astrocytic GFAP (*right*) proteins of cortical area in mouse brain sections at 30 dpi. Scale bar, 30 μ m. **e**, Quantification of percentage of Iba1⁺ (red) and GFAP⁺ (green) area in **d**. Statistical analysis in **c** and **e**, Mean \pm SD; $n = 4$; **, $p < 0.01$, Student's t -test.

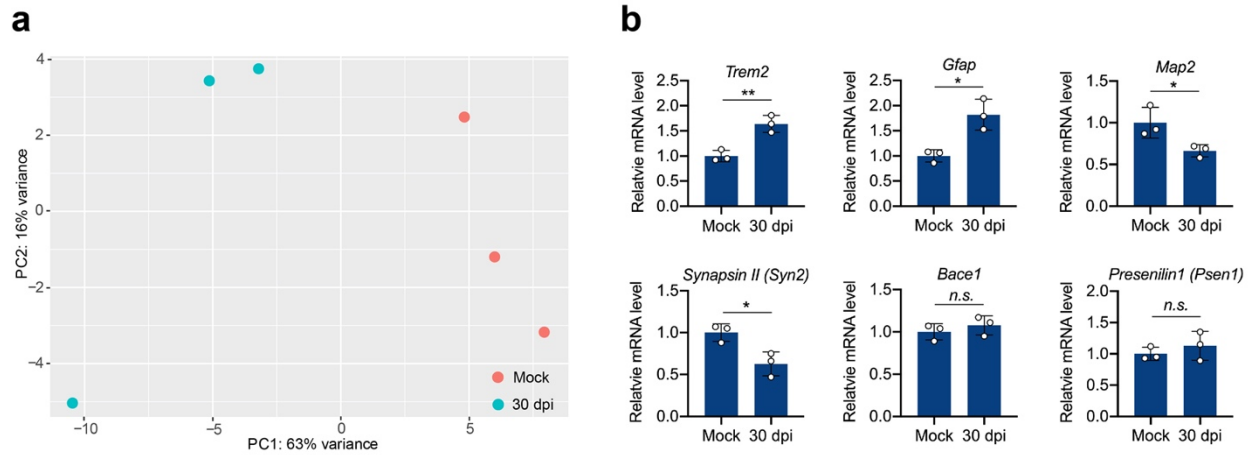


Fig. S2 Quantification of the mRNA expression in SARS-CoV-2 infected brain hippocampal tissues
a Principal component analysis of hippocampal samples from SARS-CoV-2 infected mice at 30 dpi (blue dot, $n = 3$) and uninfected mice (mock, red dot, $n = 3$) based on RNA-seq data. **b** Relative mRNA levels of *Trem2*, *Gfap*, *Map2*, *Syn2*, *Bace1* and *Psen1* in hippocampal tissues of the mice at 30 dpi. The β -actin was used as a control for normalization during qRT-PCR. Mean \pm SD; $n = 3$; *n.s.*, not significant; *, $p < 0.05$; **, $p < 0.01$, Student's *t*-test.

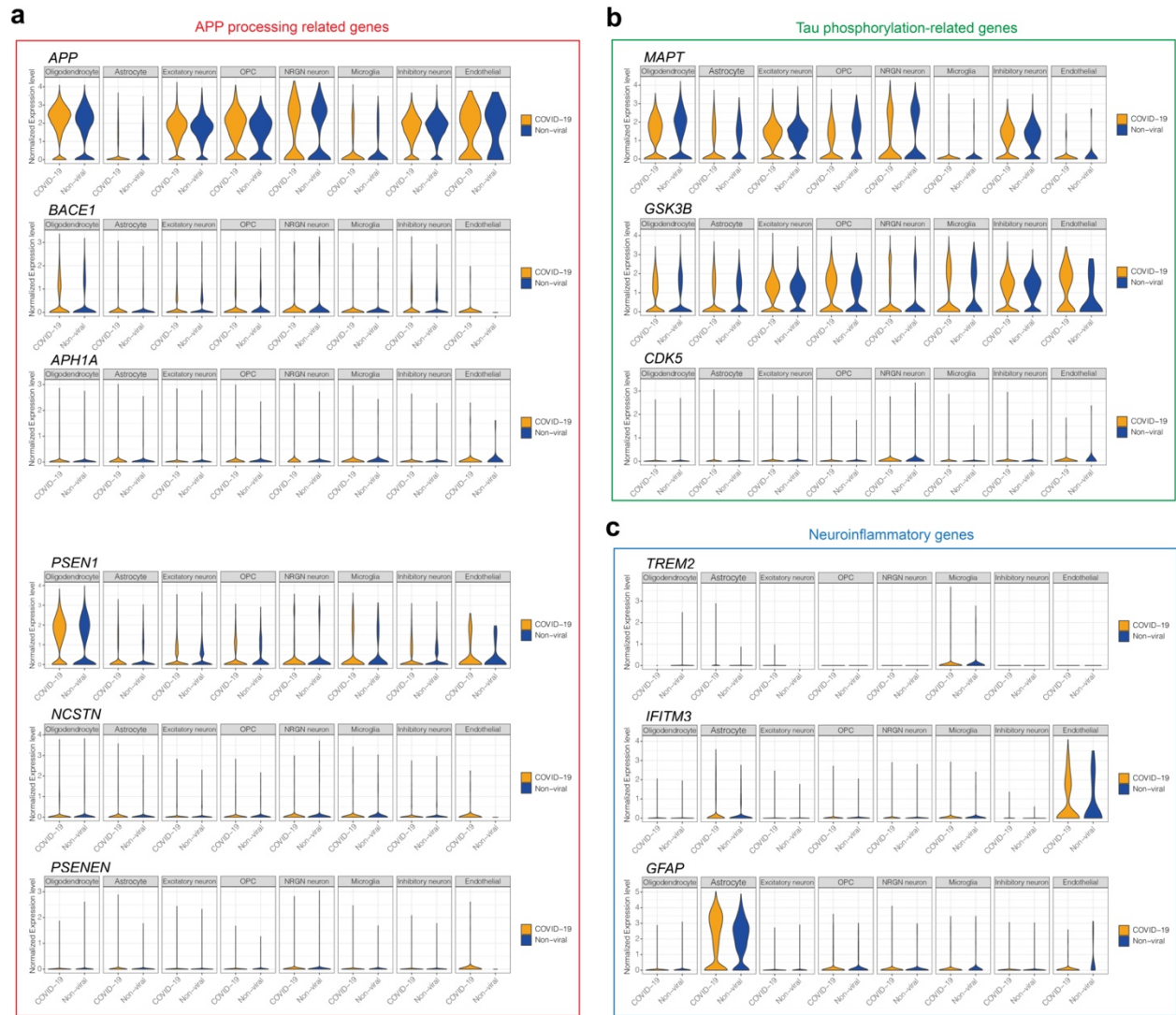


Fig. S3 Upregulation of neuroinflammatory genes and un-alteration of APP processing- and tau phosphorylation-related genes in brain cells of the COVID-19 patients
a-c The brain transcriptomic data¹³ (from single-nucleus RNA-seq) in COVID-19 patients was re-analyzed to show the expression pattern of the APP processing-related genes *APP*, *BACE1*, *APH1A*, *PSEN1*, *NCSTN* and *PSENEN* (a), tau phosphorylation-related genes *MAPT*, *GSK3B* and *CDK5* (b), and neuroinflammatory genes including *TREM2*, *IFITM3* and *GFAP* (c).

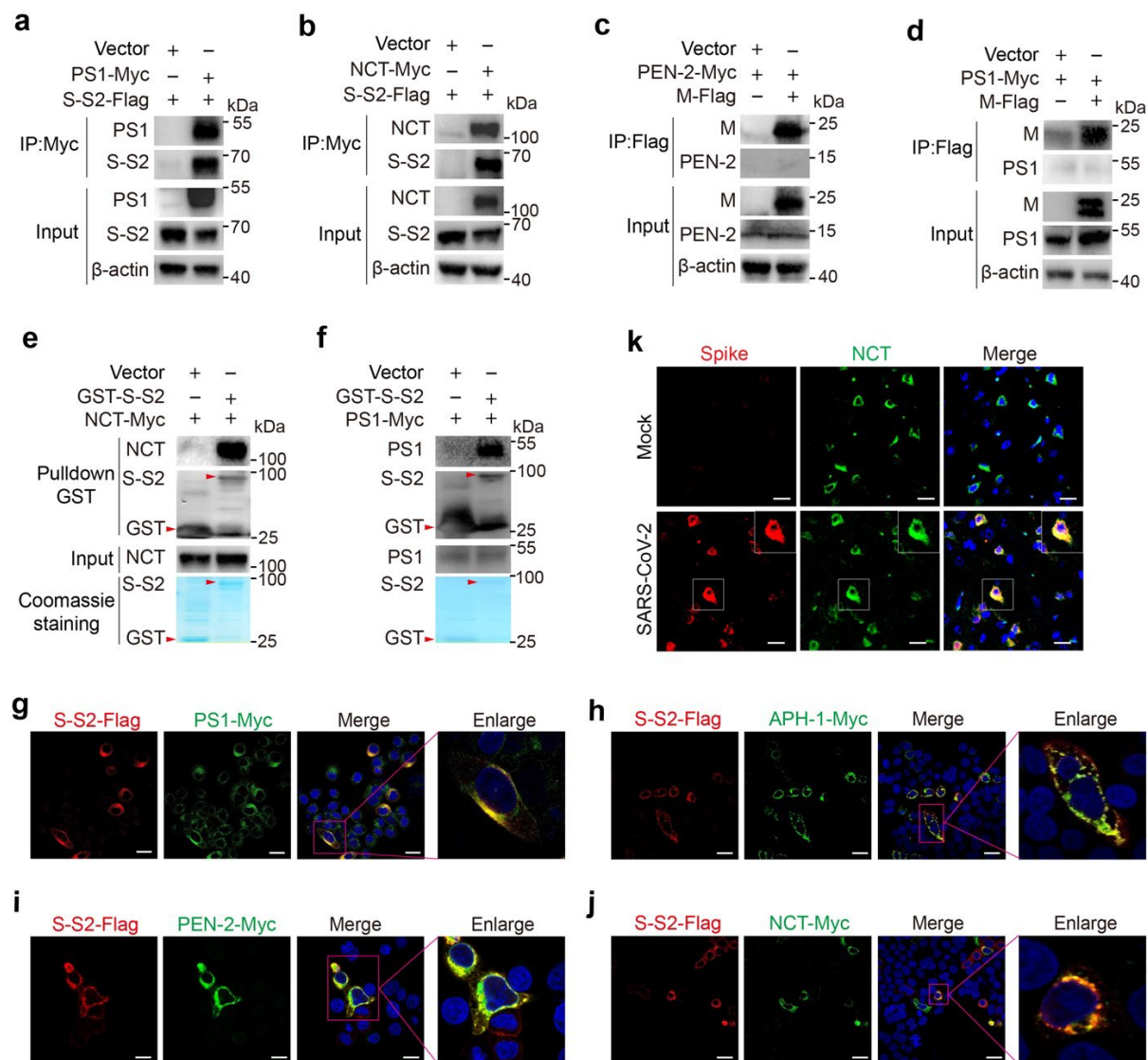


Fig. S4 SARS-CoV-2 Spike S2 subunit binds to γ -secretase

a,b co-IP assays of anti-myc monoclonal antibody in HEK293T cells transfected with myc-tagged PS1 (**a**) and myc-tagged NCT (**b**), together with flag-tagged prototyped S-S2 (S-S2-Flag) or empty vector (Vector). **c,d** co-IP assays of anti-flag monoclonal antibody in HEK293T cells transfected with flag-tagged expression vector for prototyped SARS-CoV-2 M protein (M-Flag) or empty vector (Vector), together with myc-tagged PEN-2 (**c**) or myc-tagged PS1 (**d**). **e,f** GST pull-down assays for bacterial GST (Vector) or GST-S-S2 incubated with cell lysates of HEK293T transfected with myc-tagged NCT (**e**) or PS1 (**f**). Coomassie blue staining and anti-GST and anti-myc blots were analyzed. **g-j** Representative immunofluorescence of exogenous prototyped flag-tagged S-S2 (S-S2-Flag) with myc-tagged PS1 (PS1-Myc, **g**), APH-1 (APH-1-Myc, **h**), PEN-2 (PEN-2-Myc, **i**), or NCT (NCT-Myc, **j**) in HeLa cells. Scale bar, 10 μ m. **k** Representative immunofluorescence of endogenous SARS-CoV-2 Spike and NCT proteins in cortical sections of mice with or without SARS-CoV-2 infection at 7 dpi. Scale bar, 30 μ m.

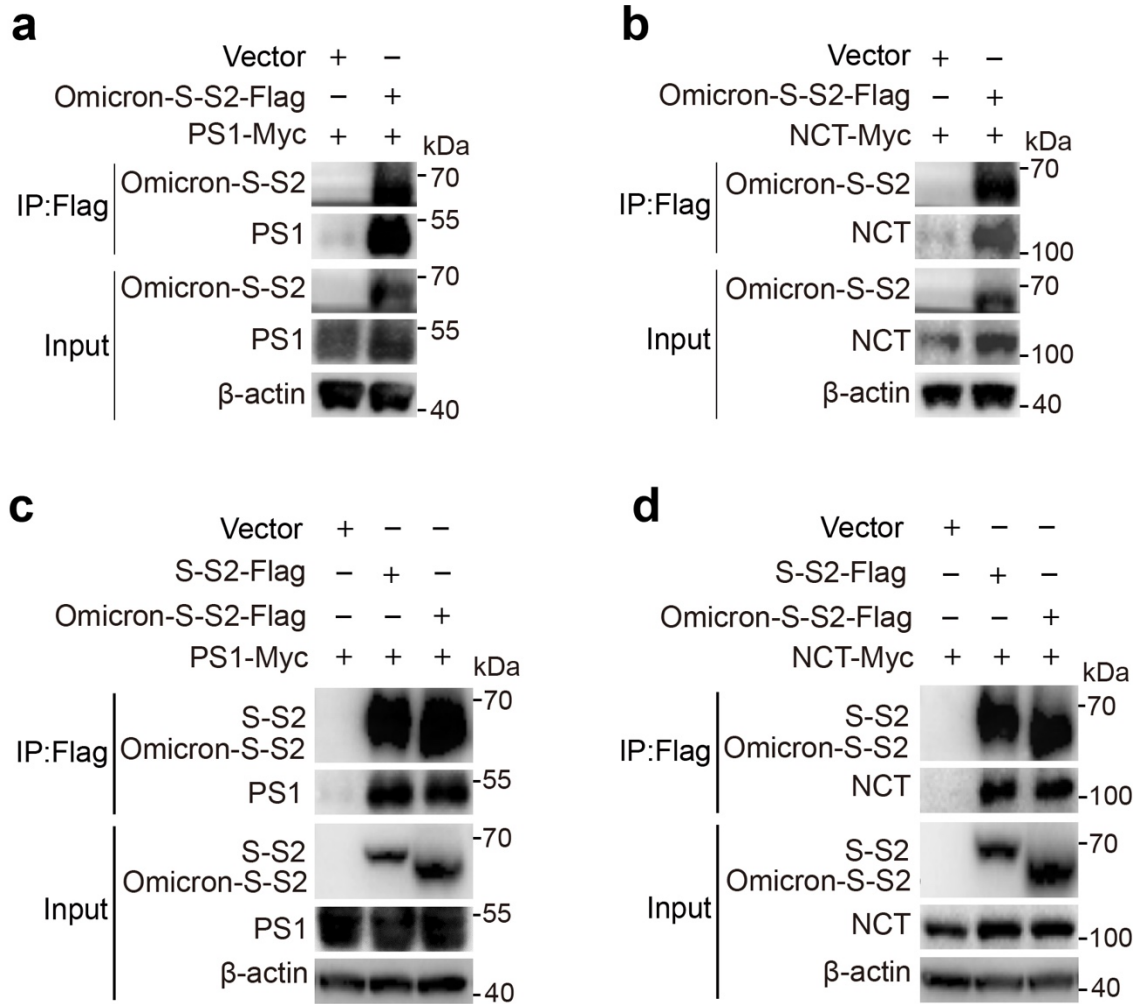


Fig. S5 Omicron Spike S2 subunit binds to γ -secretase

a,b co-IP assays of anti-flag monoclonal antibody in HEK293T cells transfected with flag-tagged Omicron Spike S2 subunit (Omicron-S-S2) or empty vector (Vector), together with myc-tagged PS1 (**a**) or NCT (**b**). **c,d** Direct comparison of the interaction of PS1 (**c**) or NCT (**d**) with S-S2 between the prototype and Omicron in same co-IP assay. Anti-flag and anti-myc blots were analyzed.

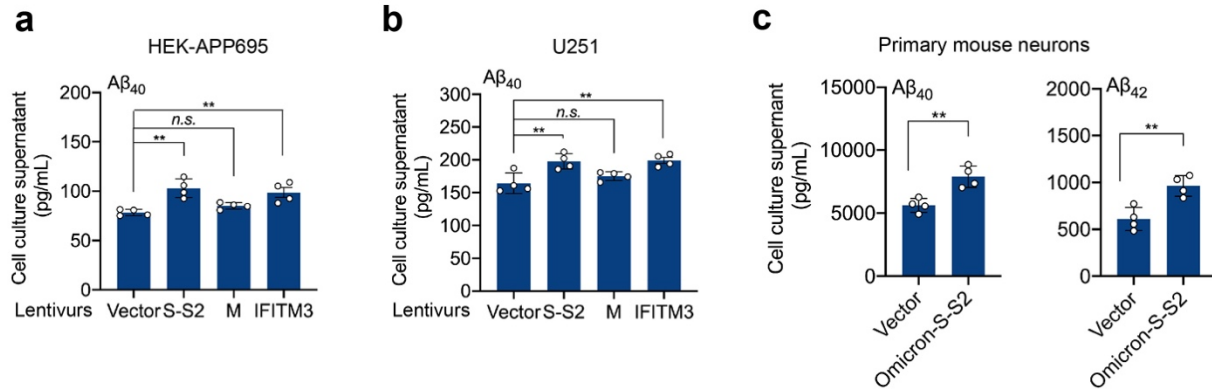


Fig. S6 Expression of SARS-CoV-2 Spike protein S2 subunit increases Aβ production

a HEK293T cells stably expressing APP695 (HEK-APP695) were transfected with expression vector for prototyped S-S2, M, or IFITM3, or empty vector (Vector) (each 0.5 μg) in 24-well plates for 36 h. **b** U251 cells were transduced with lentivirus carrying prototyped S-S2, M, or IFITM3 in 24-well plates for 36 h. The Aβ₄₀ level in the supernatants in **a** and **b** was quantified by ELISA. Mean ± SD; *n* = 4; *n.s.*, not significant; **, *p* < 0.01, one-way ANOVA with Bonferroni's *post hoc* test. **c**, Quantification of the Aβ₄₀ (*left*) and Aβ₄₂ (*right*) levels by ELISA in the supernatants of mouse primary neurons transduced with lentivirus carrying Omicron-S-S2 for 36 h or empty vector (Vector). Mean ± SD; *n* = 4; **, *p* < 0.01, Student's *t*-test.

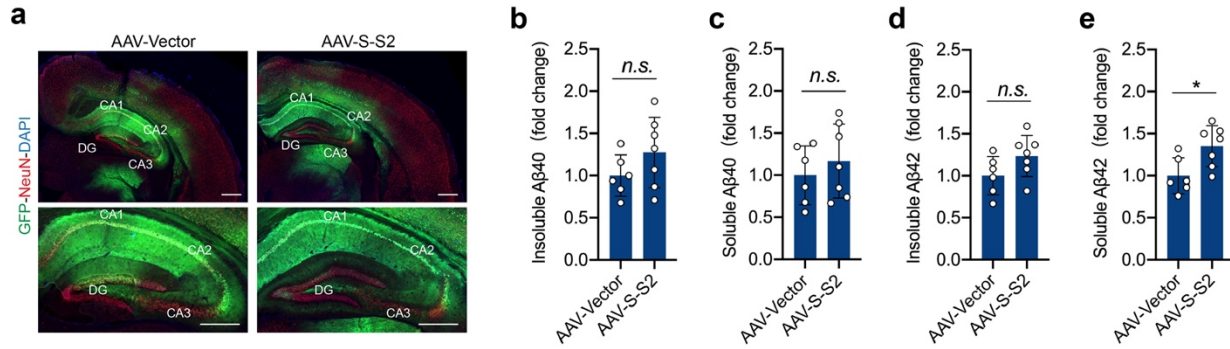


Fig. S7 Overexpression of SARS-CoV-2 Spike S2 subunit via adeno-associated virus delivery increases Aβ deposit in APP/PS1ΔE9 mice

a Fluorescence signals in brain sections of 7-month-old APP/PS1ΔE9 mice receiving AAV-Vector or AAV-S-S2 injection at age of 5 months old. Scale bar, 500 μm. **b-e** Quantification of the indicated insoluble Aβ40 and Aβ42, and soluble Aβ40 and Aβ42 in cortical tissues of the mice in **a** by ELISA. Mean ± SD; $n = 6$ or 7 ; *n.s.*, not significant; *, $p < 0.05$, Student's *t*-test.

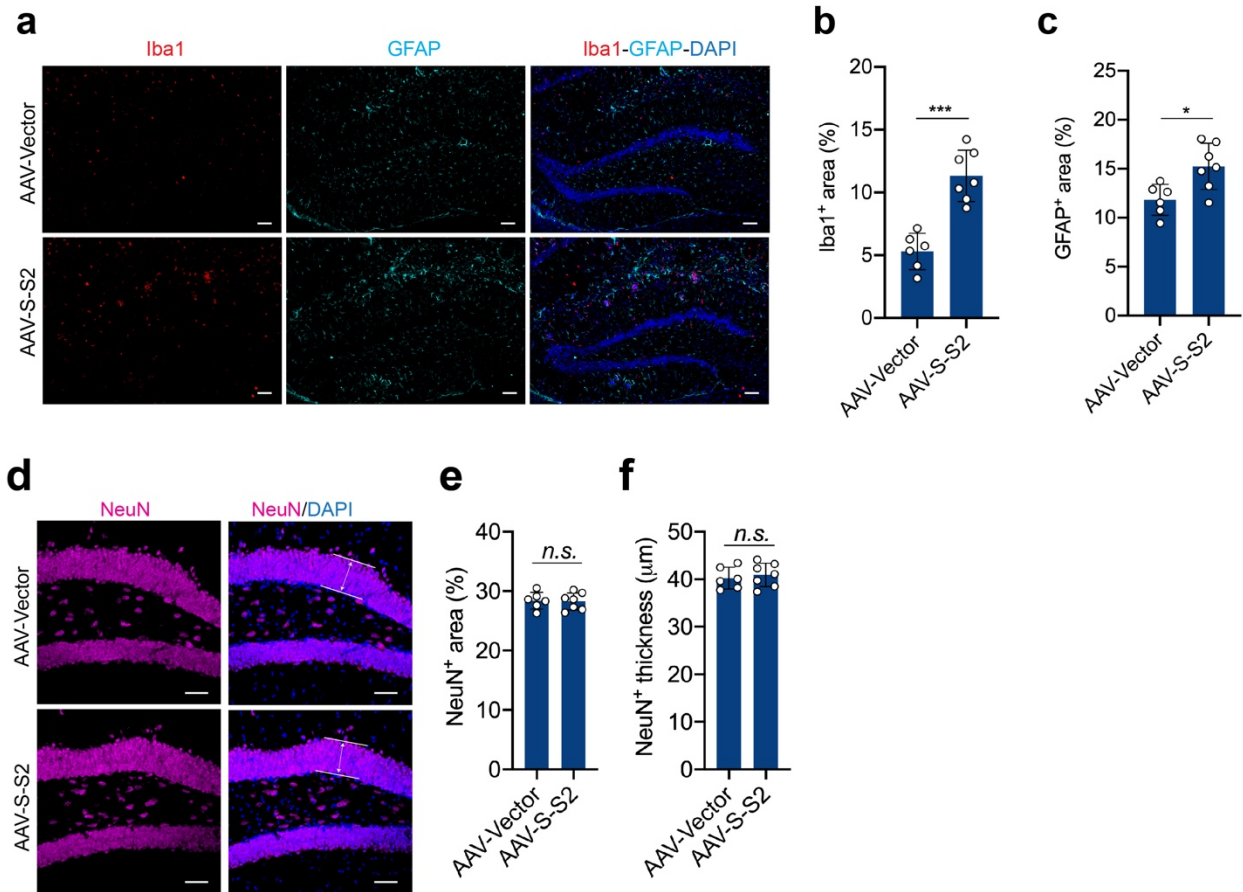


Fig. S8 Overexpression of SARS-CoV-2 Spike S2 subunit causes the activation of glial cells in APP/PS1ΔE9 mice

a Representative immunofluorescence of microglial Iba1 and astrocytic GFAP in hippocampal sections of APP/PS1ΔE9 mice with AAV delivery for SARS-CoV-2 S-S2 (AAV-S-S2) or AAV control (AAV-Vector). Scale bar, 30 μm. **b,c** Quantification of percentage of Iba1⁺ (**b**) and GFAP⁺ (**c**) area in **a**. **d** Representative immunofluorescence of NeuN protein in hippocampal sections of APP/PS1ΔE9 mice with AAV delivery for SARS-CoV-2 S-S2 (AAV-S-S2) or AAV control (AAV-Vector). Scale bar, 30 μm. **e,f** Quantification of percentage of NeuN⁺ area (**e**) and NeuN⁺ thickness (**f**) in dentate gyrus area in **d**. Each slide was used and counted for stained area via ImageJ software, and the percentage of average of stained area each section was calculated. Statistical analyses for **b**, **c**, **e** and **f**, Mean ± SD; *n* = 6 (AAV-Vector group) or *n* = 7 (AAV-S-S2 group); *n.s.*, not significant; *, *p* < 0.05; ***, *p* < 0.001, Student's *t*-test.

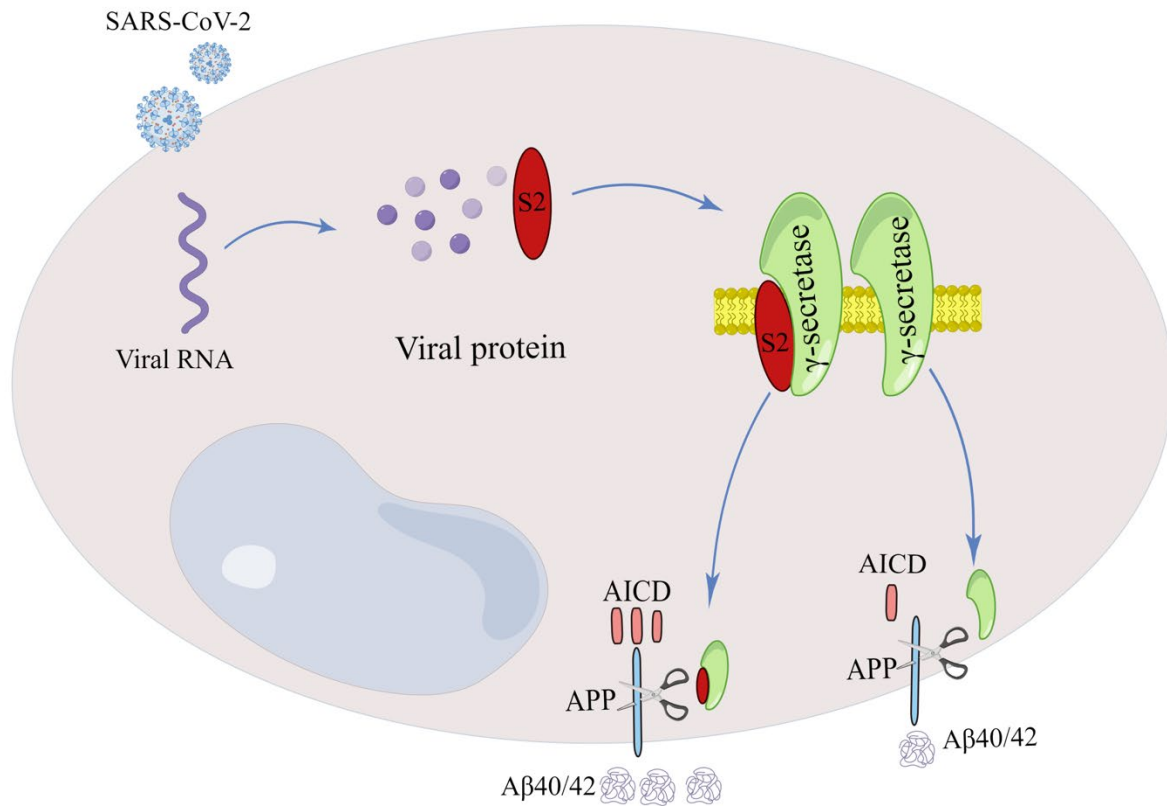


Fig. S9 Diagram showing the mechanism of the current study (by Figdraw)

Spike S2 subunit of SARS-CoV-2 infected cells interacts with γ -secretase and promotes its enzymatic cleavage of amyloid protein precursor (APP) to enhance the production of APP intracellular domain (AICD) and $A\beta$ species, which contributed to a series of downstream consequences that finally cause neural cell dysfunction and neurodegeneration.

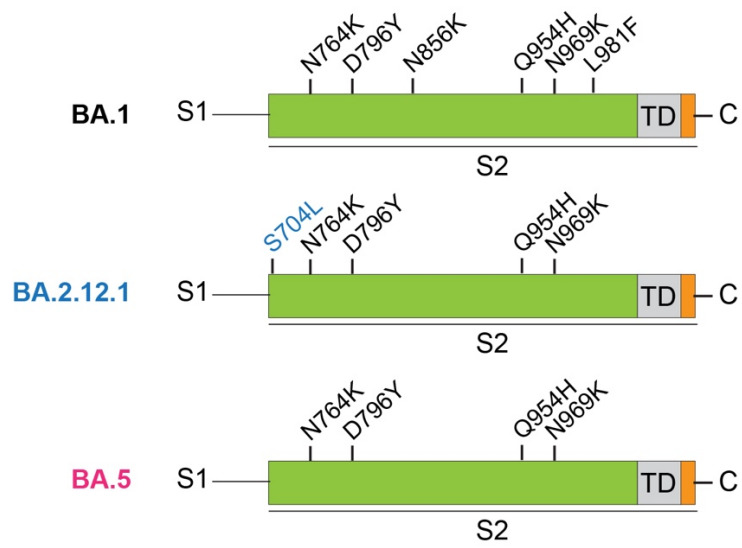


Fig. S10 Diagram showing mutations in the Spike S2 subunit of the indicated Omicron sub-variants.

Supplementary References

- 1 Zeng, J. *et al.* TRIM9-mediated resolution of neuroinflammation confers neuroprotection upon ischemic stroke in mice. *Cell Rep* **27**, 549-560, doi:10.1016/j.celrep.2018.12.055 (2019).
- 2 Song, T. Z. *et al.* Delayed severe cytokine storm and immune cell infiltration in SARS-CoV-2-infected aged Chinese rhesus macaques. *Zool Res* **41**, 503-516, doi:10.24272/j.issn.2095-8137.2020.202 (2020).
- 3 Xu, L. *et al.* COVID-19-like symptoms observed in Chinese tree shrews infected with SARS-CoV-2. *Zool Res* **41**, 517-526, doi:10.24272/j.issn.2095-8137.2020.053 (2020).
- 4 Chang, H. *et al.* Transient axonal glycoprotein-1 induces apoptosis-related gene expression without triggering apoptosis in U251 glioma cells. *Neural Regen Res* **9**, 519-525, doi:10.4103/1673-5374.130079 (2014).
- 5 Dilsizoglu Senol, A. *et al.* PAT1 inversely regulates the surface Amyloid Precursor Protein level in mouse primary neurons. *BMC Neurosci* **16**, 10, doi:10.1186/s12868-015-0152-8 (2015).
- 6 Zhang, D. F. *et al.* Complement C7 is a novel risk gene for Alzheimer's disease in Han Chinese. *Natl Sci Rev* **6**, 257-274, doi:10.1093/nsr/nwy127 (2019).
- 7 Zheng, H. Y. *et al.* Longitudinal transcriptome analyses show robust T cell immunity during recovery from COVID-19. *Sig Transduct Target Ther* **5**, 294, doi:10.1038/s41392-020-00457-4 (2020).
- 8 Bolger, A. M., Lohse, M. & Usadel, B. Trimmomatic: a flexible trimmer for Illumina sequence data. *Bioinformatics* **30**, 2114-2120, doi:10.1093/bioinformatics/btu170 (2014).
- 9 Dobin, A. *et al.* STAR: ultrafast universal RNA-seq aligner. *Bioinformatics* **29**, 15-21, doi:10.1093/bioinformatics/bts635 (2013).
- 10 Li, B. & Dewey, C. N. RSEM: accurate transcript quantification from RNA-Seq data with or without a reference genome. *Bmc Bioinformatics* **12**, 323, doi:10.1186/1471-2105-12-323 (2011).
- 11 Love, M. I., Huber, W. & Anders, S. Moderated estimation of fold change and dispersion for RNA-seq data with DESeq2. *Genome Biol* **15**, 550, doi:10.1186/s13059-014-0550-8 (2014).
- 12 Yu, G. C., Wang, L. G., Han, Y. Y. & He, Q. Y. clusterProfiler: an R Package for Comparing Biological Themes Among Gene Clusters. *Omic* **16**, 284-287, doi:10.1089/omi.2011.0118 (2012).
- 13 Yang, A. C. *et al.* Dysregulation of brain and choroid plexus cell types in severe COVID-19. *Nature* **595**, 565-571, doi:10.1038/s41586-021-03710-0 (2021).
- 14 Butler, A., Hoffman, P., Smibert, P., Papalexi, E. & Satija, R. Integrating single-cell transcriptomic data across different conditions, technologies, and species. *Nat Biotechnol* **36**, 411-420, doi:10.1038/nbt.4096 (2018).

- 15 Zeng, J. *et al.* Specific inhibition of the NLRP3 inflammasome suppresses immune overactivation and alleviates COVID-19 like pathology in mice. *eBioMedicine* **75**, 103803, doi:10.1016/j.ebiom.2021.103803 (2022).
- 16 Zeng, J. *et al.* The zika virus capsid disrupts corticogenesis by suppressing dicer activity and miRNA biogenesis. *Cell Stem Cell* **27**, 618-632, doi:10.1016/j.stem.2020.07.012 (2020).
- 17 Xie, X. C. *et al.* Emerging SARS-CoV-2 B.1.621/Mu variant is prominently resistant to inactivated vaccine-elicited antibodies. *Zool Res* **42**, 789-791, doi:10.24272/j.issn.2095-8137.2021.343 (2021).
- 18 Jankowsky, J. L. *et al.* Mutant presenilins specifically elevate the levels of the 42 residue beta-amyloid peptide in vivo: evidence for augmentation of a 42-specific gamma secretase. *Hum Mol Genet* **13**, 159-170, doi:10.1093/hmg/ddh019 (2004).
- 19 Luo, R. *et al.* A novel missense variant in ACAA1 contributes to early-onset Alzheimer's disease, impairs lysosomal function, and facilitates amyloid-beta pathology and cognitive decline. *Signal Transduct Target Ther* **6**, 325, doi:10.1038/s41392-021-00748-4 (2021).
- 20 Luo, R. *et al.* Activation of PPARA-mediated autophagy reduces Alzheimer disease-like pathology and cognitive decline in a murine model. *Autophagy* **16**, 52-69, doi:10.1080/15548627.2019.1596488 (2020).
- 21 Piller, C. Blots on a field? *Science* **377**, 358-363, doi:10.1126/science.add9993 (2022).
- 22 Zott, B. *et al.* A vicious cycle of beta amyloid-dependent neuronal hyperactivation. *Science* **365**, 559-565, doi:10.1126/science.aay0198 (2019).
- 23 Pascoal, T. A. *et al.* Microglial activation and tau propagate jointly across Braak stages. *Nat Med* **27**, 1592-1599, doi:10.1038/s41591-021-01456-w (2021).
- 24 Karran, E. & De Strooper, B. The amyloid hypothesis in Alzheimer disease: new insights from new therapeutics. *Nat Rev Drug Discov* **21**, 306-318, doi:10.1038/s41573-022-00391-w (2022).
- 25 Palop, J. J. & Mucke, L. Amyloid-beta-induced neuronal dysfunction in Alzheimer's disease: from synapses toward neural networks. *Nat Neurosci* **13**, 812-818, doi:10.1038/nn.2583 (2010).